Effects of Contact-Line Pinning on the Adsorption of Nonspherical Colloids at Liquid Interfaces

Anna Wang,[1] W. Benjamin Rogers,[1,2] and Vinothan N. Manoharan[1,3,*]
[1]Harvard John A. Paulson School of Engineering and Applied Sciences, Harvard University, Cambridge, Massachusetts 02138, USA
[2]Martin Fisher School of Physics, Brandeis University, Waltham, Massachusetts 02453, USA
[3]Department of Physics, Harvard University, Cambridge, Massachusetts 02138, USA
(Received 13 July 2016; revised manuscript received 9 August 2017; published 7 September 2017)

The effects of contact-line pinning are well known in macroscopic systems but are only just beginning to be explored at the microscale in colloidal suspensions. We use digital holography to capture the fast three-dimensional dynamics of micrometer-sized ellipsoids breaching an oil-water interface. We find that the particle angle varies approximately linearly with the height, in contrast to results from simulations based on the minimization of the interfacial energy. Using a simple model of the motion of the contact line, we show that the observed coupling between translational and rotational degrees of freedom is likely due to contact-line pinning. We conclude that the dynamics of colloidal particles adsorbing to a liquid interface are not determined by the minimization of interfacial energy and viscous dissipation alone; contact-line pinning dictates both the time scale and pathway to equilibrium.

DOI: 10.1103/PhysRevLett.119.108004

The adsorption of a microscopic colloidal particle to a liquid interface is a dynamic wetting process: In the reference frame of the particle, the three-phase contact line moves along the particle's surface. Our understanding of analogous wetting processes in macroscopic systems is based on two types of models: those that relate the motion of the contact line to the viscous dissipation in the fluid "wedge" bounded by the solid and the liquid interface [1–3] and those that consider dissipation local to the contact line [4,5]. Models in this second class treat the motion of the contact line as a thermally activated process, in which the contact line transiently pins on nanoscale defects and hops between them. The two viewpoints are not incompatible: Both types of dissipation can be relevant to experiments [6], and thermally activated motion of the contact line can be viewed as a model for how slip occurs at the solid boundary [7]. The nanoscale defects responsible for pinning the contact line are now understood to be important in macroscopic wetting experiments at a small capillary number [7–9] and in phenomena related to contact-angle hysteresis [10].

Such defects—and the associated hopping of the contact line—have also proven important for understanding the dynamics of microscopic colloidal particles at liquid interfaces. These particles can strongly adhere to the interface, owing to the large change in the total interfacial energy of the system once the particles bind [11]. The resulting systems are used to study phase transitions and self-assembly in two dimensions [12–18], to fabricate new materials [19–21], and to formulate Pickering emulsions and colloidosomes [22–25]. But nearly all particles used in such systems have nanoscale surface features that can pin the contact line [26]. Whereas strong pinning sites can affect interactions [27] and motion on curved interfaces [28], even weak pinning sites can dramatically affect dynamics. For example, Boniello and co-workers [29] showed that the in-plane diffusion of particles straddling an air-water interface is inconsistent with models of viscous drag in the bulk fluids but consistent with models of contact-line fluctuations caused by nanoscale defects. Also, Kaz, McGorty, and co-workers [30] showed that spherical colloidal particles breaching liquid interfaces relax toward equilibrium at a rate orders of magnitude slower than that predicted by models of viscous dissipation in a fluid wedge. Dynamic wetting models based on thermally activated hopping [4,31] fit the observed adsorption trajectories well over a wide range of time scales.

Here we examine the effects of transient pinning and depinning on the *pathway* that ellipsoidal colloidal particles take to equilibrium and not just the time required to get there. By "pathway," we mean the way in which the degrees of freedom vary with time. For example, a spherical particle has one degree of freedom—its height relative to the interface. Its pathway to equilibrium does not depend on pinning effects: At a low Reynolds number, the height changes monotonically with time, regardless of whether the contact line becomes pinned along the way. By contrast, an ellipsoid of revolution, or spheroid, has two degrees of freedom—its center-of-mass position and orientation—which need not vary monotonically with time. In fact, molecular dynamics [32] and Langevin dynamics studies [33] predict that both the height and orientation of ellipsoidal particles breaching an interface vary nonmonotonically with time [Fig. 1(a)]. These simulations assume

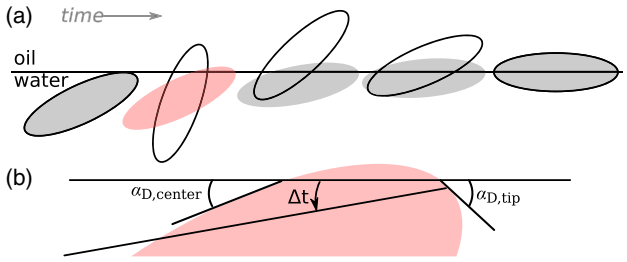

FIG. 1. (a) Schematic showing the cross section through the long axis of an ellipsoidal particle breaching an interface. Simulations assuming the interfacial energy is minimized at each time step predict trajectories (solid lines) that are nonmonotonic in both the center-of-mass position and polar angle [32,33]. Our experimental results (shaded ellipses) show a monotonic increase in both the height and polar angle. See also the movie in Supplemental Material [36]. (b) Schematic of contact-line motion for one scenario in (a). A line shows where the contact line moves in the frame of reference of the particle after time Δt. The dynamic contact angles at two points are shown.

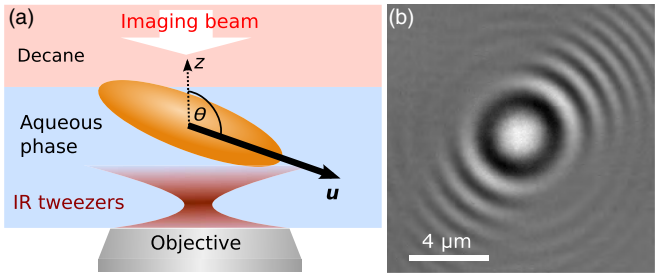

FIG. 2. Schematic of the experimental setup. (a) The sample is illuminated with a red collimated laser ($\lambda = 660$ nm). A counter-propagating infrared laser ($\lambda = 785$ nm) is used to gently push the particles against gravity toward the interface. In the coordinate system used here, the imaging axis lies along z, and the interface is at $z = 0$. The center-of-mass position and the polar angle θ of the particle are defined relative to the laboratory frame by a unit vector $\mathbf{u}$ that points along the long axis of the ellipsoid. (b) A typical hologram of an ellipsoid at an interface. See also the movie in Supplemental Material [36].

that the particles follow a quasistatic approach to equilibrium, such that the total interfacial energy is minimized at each step along the way, and they do not model contact-line pinning. They predict an equilibration time of 10 μs based on the viscous dissipation, but previous experimental studies of prolate spheroids at interfaces by Coertjens *et al.* [34] and Mihiretie [35] suggest that the equilibration time is much longer, hinting at pinning effects.

We use a fast 3D imaging technique, digital holographic microscopy, to observe ellipsoidal (prolate spheroidal) colloidal particles adsorbing to an oil-water interface. We find that not only is the equilibration time orders of magnitude larger than that predicted by simulations, but the position and orientation of the particle vary *monotonically* with time, in contrast to the nonmonotonic pathways found in simulations [32,33]. Interestingly, the center-of-mass position and the polar angle of the particle are coupled, so that the particle "rolls" into its equilibrium position as if it were subject to a tangential frictional force [Fig. 1(a) and Supplemental Material [36]]. We argue that these effects are due to contact-line pinning.

To make ellipsoidal particles, we heat 1.0-μm-diameter sulfate-functionalized polystyrene particles (Invitrogen) above their glass transition temperature and stretch them [36]. Using the apparatus shown in Fig. 2, we capture holograms of individual ellipsoids at 100 frames per second as they approach an interface between decane and a water-glycerol mixture. The holograms encode the three-dimensional position and orientation of the particle in the spacing and shape of the interference fringes. We extract this information, along with the particle size and refractive index, by fitting a T-matrix model [45] of the scattering from the particles to our data [36].

We find that the particles relax to equilibrium slowly, despite some abrupt motion along the way, as shown in Fig. 3(a). After 1 s, or 5 orders of magnitude longer than the equilibrium time observed in simulations [33], the particles are still not equilibrated. Furthermore, their height scales roughly linearly with the logarithm of the elapsed time after the breach. Because this is the same scaling observed by Kaz and co-workers [30], the likely origin of the slow dynamics is contact-line pinning and depinning, the same mechanism observed in spherical particles. The slow dynamics are perhaps unsurprising, since the particles are stretched versions of those used by Kaz *et al.* [30].

More surprisingly, we find that the abrupt changes in height [Fig. 3(a)] correlate with abrupt changes in the polar angle θ [Fig. 3(b)]. Indeed, when we examine θ as a function of z, we find that the relationship is approximately linear [Fig. 3(c)]. Furthermore, although the particles approach the interface from a variety of different polar angles, the θ-z plots form lines with similar slopes, hinting at the presence of a dynamical attractor.

The linear relationship between θ and z is reminiscent of rolling, where translation and rotation are coupled by friction. The particles "pivot" into the interface, as shown by the rendering of individual points along the observed trajectories [Fig. 1(a) and Supplemental Material [36]]. In contrast, the simulations by Günther, Frijters, and Harting [32] and de Graaf, Dijkstra, and van Roij [33] predict that θ and z should vary nonmonotonically with time [Fig. 1(a)].

We therefore seek a different model to explain the observed rotational-translational coupling, one that takes into account contact-line pinning. We adopt the viewpoint of Kaz *et al.* [30] and assume that the contact line pins to defects on the surface of the particle and hops between pinning sites with the aid of thermal kicks. We calculate the velocity of the contact line using an Arrhenius equation coupled to a model for the force, determined by the dynamic contact angle $\alpha_D(t)$. In contrast to the model for spheres, our model allows $\alpha_D(t)$ to vary as a function of

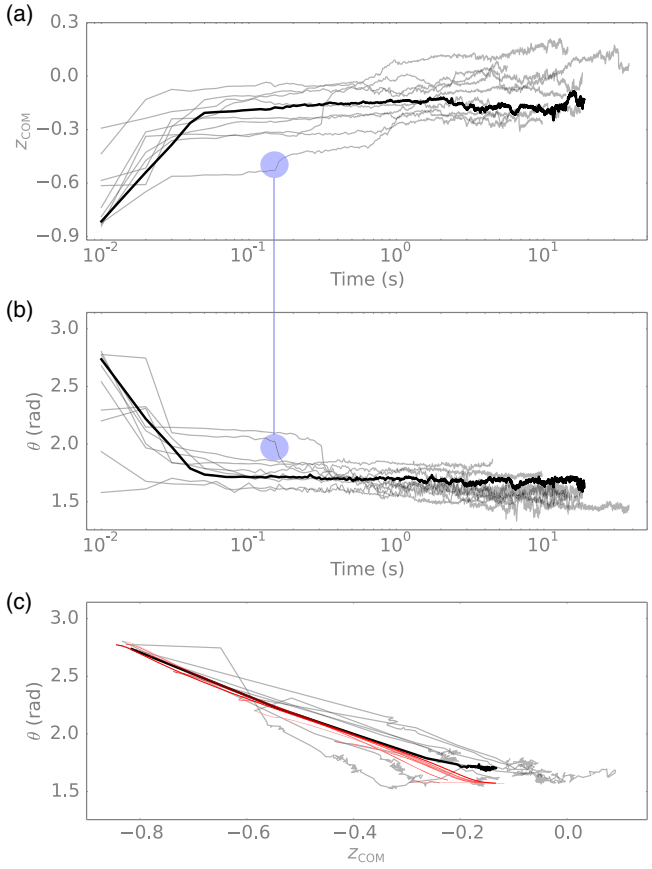

FIG. 3. The height (a) and polar angle θ (b) of ellipsoids after they breach (breach at $t = 0$ s) appear correlated (example marked with blue circles). To compare data from particles of different aspect ratios on the same plot, we normalize the center-of-mass height relative to the interface [33] to obtain $z_{\mathrm{COM}} = z/\sqrt{2a^2 + b^2}$, where a and b are the semiminor and semimajor axes of the spheroid. (c) The polar angle varies with the height. Our model (red), based on contact-line hopping over defects, produces almost linear relationships between z and θ for the particles from the experiments.

the position on the particle, though we still assume that the interface remains flat at all times, a simplification that we justify based on the energetic cost of bending the interface.

For a horizontal interface defined by a denser aqueous phase on the bottom and an oil phase on top (Fig. 2), the force on each segment of the contact line is determined from the imbalance between the three interfacial tensions (oil-water σ_{ow}, particle-water σ_{pw}, and particle-oil σ_{po}):

$$\begin{aligned} F_{\mathrm{CL}} &= \sigma_{ow}\cos\alpha_D(t) + \sigma_{pw} - \sigma_{po} \\ &= \sigma_{ow}[\cos\alpha_D(t) - \cos\alpha_E], \end{aligned} \tag{1}$$

where α_E is the equilibrium contact angle. To understand this relation, consider Fig. 1(b). The force is tangent to the particle. Because the contact angle is defined relative to the aqueous phase, F_{CL} is positive and the contact line moves *down* the particle (in the particle frame) if the particle approaches the interface from the aqueous phase ($\alpha_D < \alpha_E$). If the particle approaches the interface from the oil phase ($\alpha_D > \alpha_E$), F_{CL} is negative and the contact line moves *up* the particle. Because the particle is nonspherical, the force per unit length along the contact line is asymmetric about the short axis of the ellipsoid unless the particle breaches the interface at exactly $\theta = \pi/2$.

The direction and magnitude of this force determine the velocity of the contact line along the particle surface. We relate F_{CL} to the velocity of the contact line using an Arrhenius equation that is valid when forward hops dominate [4,30] ($|\alpha_E - \alpha_D| \gtrsim 0.01$, as discussed in Supplemental Material [36]):

$$V = \frac{F_{\mathrm{CL}}(t)}{|F_{\mathrm{CL}}(t)|} V_0 \exp\left(-\frac{U}{kT} + \frac{|F_{\mathrm{CL}}(t)|A}{2kT}\right), \tag{2}$$

where V is the velocity of the contact line tangent to the particle, V_0 is a molecular velocity scale, A is the area per defect on the surface of the particle, and U is the energy with which each defect pins the contact line. When spherical particles start in the aqueous phase, Eq. (2) reduces to the form described in the Supplemental Information of Kaz *et al.* [30]. Further details of the model are given in Supplemental Material [36].

Before comparing the model to the data, we first determine which parameters in the model control the trajectory. The dynamic contact angle is greater near the tips of the particle than it is near the center ($\alpha_{D,\mathrm{tip}} > \alpha_{D,\mathrm{center}}$), as illustrated in Fig. 1(b). The part of the contact line nearest the tip travels more slowly than the part nearest the center [$V_{\mathrm{tip}} < V_{\mathrm{center}}$ according to Eqs. (1) and (2)], leading to the observed pivoting motion. Considering only these two points, the ratio $V_{\mathrm{center}}/V_{\mathrm{tip}} = \exp[\sigma_{ow}A(\cos\alpha_{D,\mathrm{center}} - \cos\alpha_{D,\mathrm{tip}})/2kT]$ approximates the rate at which z and θ change relative to each other. We therefore expect the shape and aspect ratio of the particle, which determine the values of α_D for a given θ and z, and the area per defect A to control the form of the θ-z curve. Changing the size of the particle, U, or α_E alters how θ and z depend on time but not how θ and z evolve with each other. We explore the effect of particle shape further below.

The model produces trajectories that agree with experimental observations. In Fig. 3(c), we plot calculated θ-z trajectories for each of the particles using the measured aspect ratio determined from fitting the holograms and a defect area equal to that measured in Kaz *et al.* [30], $A = 4$ nm^2. We have strong evidence that A is nanoscale, as discussed in Supplemental Material [36]. The modeled θ and z are both monotonic with time, in contrast to the predictions from earlier simulations. Moreover, θ varies linearly with z, reproducing the translational-rotational coupling in our experimental results. The slope predicted

by the model (-1.75 ± 0.16 rad) agrees with the average slope in our experimental results (-1.64 ± 0.76 rad).

Our model predicts that all trajectories collapse onto one line for a given A [Fig. 3(c)]. de Graaf and co-workers found a similar "dynamical attractor" for ellipsoids in their Langevin simulations [33], while Günther, Frijters, and Harting [32] found that the adsorption trajectory depends sensitively on the angle of the particle when it first touches the interface. Our model predicts an attractor, but the attractor arises from the pinning and, in particular, from how pinning ensures that the contact-line velocity near the tip is always smaller than that near the center.

The only discrepancy between the model and our data is that the slopes of the modeled trajectories are more narrowly distributed than the experimentally observed slopes. This discrepancy may be due to deviations in shape from perfect prolate spheroids (see the image of the particles in Supplemental Material [36]), which would affect the curvature of the particle and hence α_D. The area per defect A might also vary between particles. Our data fall between the calculated attractors for particles with $A = 1$ and 30 nm^2. Finally, the stretching of the particles might lead to an inhomogeneous defect density, which we do not account for in our model. However, the agreement between the average observed and calculated slopes suggests that our assumption of a uniform defect density is valid to within the uncertainties of our measurements [36].

Our model further predicts that if the particles were spherical, there would be no net torque on the particle, owing to the symmetry. To verify this prediction, we examine spherocylindrical particles (Fig. 4), each of which consists of a cylinder with hemispherical caps. If the spherocylinder is hydrophilic, such that a sphere of the same material has an equilibrium contact angle smaller than $\pi/4$ [Fig. 4(a)], it can attach to the interface at a range of polar angles all having the same energy [Fig. 4(a)]. Our model predicts that the contact line will not exert a torque on the particle and that the particle should therefore remain at the same polar angle.

Indeed, we observe that when hydrophilic spherocylinders breach the interface, their polar angles remain fixed, although their azimuthal angles can still fluctuate [Fig. 4(b)]. The absence of equilibration is surprising, because the minimum-energy configuration for spherocylinders is $\theta = \pi/2$. However, the observed trajectories agree with the prediction of our model.

We therefore conclude that accounting for contact-line pinning, and not just interfacial energy, is necessary to understand the dynamics of nonspherical particles at liquid interfaces. The slow relaxation observed in such systems is just one manifestation of the pinning; as we have shown here, the pinning can also alter the pathway to equilibrium. The agreement between the model and experiment suggests that the pathway is controlled not only by the size of the defects on the solid surfaces but also by the local curvature

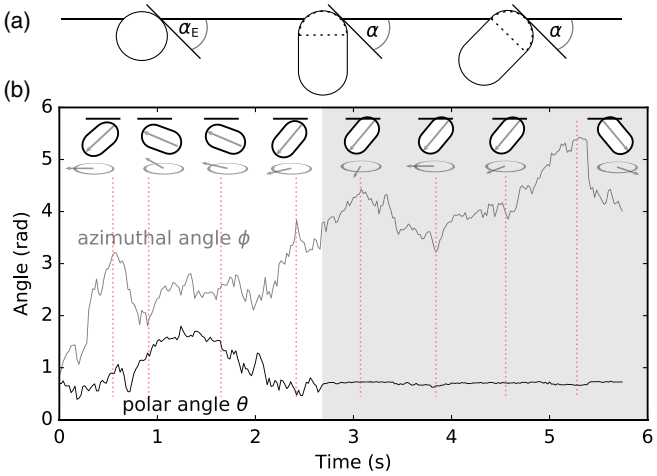

FIG. 4. (a) A hydrophilic spherocylinder ($\alpha_E < \pi/4$; hemispherical caps drawn in dotted lines) can reach a local minimum in the interfacial energy when the contact angle $\alpha = \alpha_E$. (b) Experimental data showing that a hydrophilic silica spherocylinder freely rotates about the z axis once it has attached to the interface (shaded region), but its polar angle remains fixed. Arrows indicate the particle's polar and azimuthal angles at the time points indicated by the red dotted lines.

of the particle. Thus, not only is the road to equilibrium long, but it also depends on the details of the shape of the particle.

These results have practical implications for assembling particles at an interface and, at the same time, lead to a new fundamental understanding of how dynamic wetting influences particles at interfaces. In terms of practical implications, the unexpectedly long adsorption times we find in our experiments might significantly affect the aging of Pickering emulsions. Although we have neglected the curvature of the interface in our simple dynamical model, ellipsoidal particles should induce a quadrupolar capillary field in equilibrium [46]. Therefore, the equilibration of multiple particles at the interface might be complicated by the slowly evolving capillary interactions between them. Also, the shape of the particle might play a large role in determining if and how such systems arrive at equilibrium. Particles like the spherocylinder (and related particles such as *E. coli* and other pill-shaped bacteria) can get stuck at a particular angle after attaching to the interface, because the contact line "sees" a sphere [Fig. 4(a)]. Such particles would therefore need a large thermal fluctuation to rotate toward their equilibrium configuration.

In terms of fundamental understanding, the ability of our model to recreate the nearly linear θ-z adsorption trajectories for ellipsoids validates the idea that contact-line pinning couples orientational and translational degrees of freedom. The role that pinning plays is akin to the role of friction in rolling. Here, however, the friction arises not from the interactions between microscopic features on two solid surfaces but from the interactions between nanoscale

defects on a solid surface and a deformable liquid-liquid interface. Though these interactions are weak enough to be disrupted by thermal fluctuations and the capillary driving forces are large, the frictional coupling can nonetheless drive adsorption trajectories that are observably different from those expected from interfacial energy minimization and viscous dissipation.

We thank Thomas E. Kodger and Peter J. Yunker for their apparatus and advice for making ellipsoids, Michael I. Mishchenko for allowing us to incorporate his T-matrix code with our hologram analysis software HoloPy, Christopher Chan Miller for help with adapting Fortran code for use with HoloPy, and Kundan Chaudhary for synthesizing the silica spherocylinders. This work was funded by the National Science Foundation (NSF) through Grant No. DMR-1306410 and by the Harvard MRSEC through NSF Grant No. DMR-1420570.

*vnm@seas.harvard.edu

[1] C. Huh and L. E. Scriven, J. Colloid Interface Sci. **35**, 85 (1971).
[2] E. B. Dussan V. and S. H. Davis, J. Fluid Mech. **65**, 71 (1974).
[3] P. G. de Gennes, Rev. Mod. Phys. **57**, 827 (1985).
[4] T. D. Blake and J. M. Haynes, J. Colloid Interface Sci. **30**, 421 (1969).
[5] T. D. Blake, J. Colloid Interface Sci. **299**, 1 (2006).
[6] F. Brochard-Wyart and P. G. de Gennes, Adv. Colloid Interface Sci. **39**, 1 (1992).
[7] J. H. Snoeijer and B. Andreotti, Annu. Rev. Fluid Mech. **45**, 269 (2013).
[8] A. Prevost, E. Rolley, and C. Guthmann, Phys. Rev. Lett. **83**, 348 (1999).
[9] E. Rolley and C. Guthmann, Phys. Rev. Lett. **98**, 166105 (2007).
[10] A. Giacomello, L. Schimmele, and S. Dietrich, Proc. Natl. Acad. Sci. U.S.A. **113**, E262 (2016).
[11] B. P. Binks and T. S. Horozov, *Colloidal Particles at Liquid Interfaces* (Cambridge University Press, Cambridge, 2006).
[12] P. Pieranski, Phys. Rev. Lett. **45**, 569 (1980).
[13] R. Aveyard, J. H. Clint, D. Nees, and V. N. Paunov, Langmuir **16**, 1969 (2000).
[14] K. Zahn and G. Maret, Phys. Rev. Lett. **85**, 3656 (2000).
[15] A. R. Bausch, M. J. Bowick, A. Cacciuto, A. D. Dinsmore, M. F. Hsu, D. R. Nelson, M. G. Nikolaides, A. Travesset, and D. A. Weitz, Science **299**, 1716 (2003).
[16] H. König, R. Hund, K. Zahn, and G. Maret, Eur. Phys. J. E **18**, 287 (2005).
[17] M. Cavallaro, L. Botto, E. P. Lewandowski, M. Wang, and K. J. Stebe, Proc. Natl. Acad. Sci. U.S.A. **108**, 20923 (2011).
[18] L. Botto, L. Yao, R. L. Leheny, and K. J. Stebe, Soft Matter **8**, 4971 (2012).
[19] V. Paunov and O. Cayre, Adv. Mater. **16**, 788 (2004).
[20] M. Retsch, Z. Zhou, S. River, M. Kappl, X. S. Zhao, U. Jonas, and Q. Li, Macromol. Chem. Phys. **210**, 230 (2009).
[21] L. Isa, K. Kumar, M. Mller, J. Grolig, M. Textor, and E. Reimhult, ACS Nano **4**, 5665 (2010).
[22] W. Ramsden, Proc. R. Soc. London **72**, 156 (1903).
[23] S. U. Pickering, J. Chem. Soc. **91**, 2001 (1907).
[24] A. Dinsmore, M. F. Hsu, M. Nikolaides, M. Marquez, A. Bausch, and D. Weitz, Science **298**, 1006 (2002).
[25] R. McGorty, J. Fung, D. Kaz, and V. N. Manoharan, Mater. Today **13**, 34 (2010).
[26] A. Wang, R. McGorty, D. M. Kaz, and V. N. Manoharan, Soft Matter **12**, 8958 (2016).
[27] P. A. Kralchevsky, N. D. Denkov, and K. D. Danov, Langmuir **17**, 7694 (2001).
[28] N. Sharifi-Mood, I. B. Liu, and K. J. Stebe, Soft Matter **11**, 6768 (2015).
[29] G. Boniello, C. Blanc, D. Fedorenko, M. Medfai, N. B. Mbarek, M. In, M. Gross, A. Stocco, and M. Nobili, Nat. Mater. **14**, 908 (2015).
[30] D. M. Kaz, R. McGorty, M. Mani, M. P. Brenner, and V. N. Manoharan, Nat. Mater. **11**, 138 (2012).
[31] C. E. Colosqui, J. F. Morris, and J. Koplik, Phys. Rev. Lett. **111**, 028302 (2013).
[32] F. Günther, S. Frijters, and J. Harting, Soft Matter **10**, 4977 (2014).
[33] J. de Graaf, M. Dijkstra, and R. van Roij, J. Chem. Phys. **132**, 164902 (2010).
[34] S. Coertjens, P. Moldenaers, J. Vermant, and L. Isa, Langmuir **30**, 4289 (2014).
[35] B. Mihiretie, Ph.D. thesis, Université de Bordeaux 1, 2013.
[36] See Supplemental Material at http://link.aps.org/supplemental/10.1103/PhysRevLett.119.108004, which includes Refs. [37–44], for details of sample preparation, analysis methods, and movies.
[37] C. Ho, A. Keller, J. Odell, and R. Ottewill, Colloid Polym. Sci. **271**, 469 (1993).
[38] P. J. Yunker, T. Still, M. A. Lohr, and A. G. Yodh, Nature (London) **476**, 308 (2011).
[39] K. Chaudhary, Q. Chen, J. J. Juárez, S. Granick, and J. A. Lewis, J. Am. Chem. Soc. **134**, 12901 (2012).
[40] A. Kuijk, A. van Blaaderen, and A. Imhof, J. Am. Chem. Soc. **133**, 2346 (2011).
[41] B. Ovryn and S. H. Izen, J. Opt. Soc. Am. A **17**, 1202 (2000).
[42] M. A. Yurkin and A. G. Hoekstra, J. Quant. Spectrosc. Radiat. Transfer **112**, 2234 (2011).
[43] A. Wang, T. G. Dimiduk, J. Fung, S. Razavi, I. Kretzschmar, K. Chaudhary, and V. N. Manoharan, J. Quant. Spectrosc. Radiat. Transfer **146**, 499 (2014).
[44] T. M. Kreis, Opt. Eng. **41**, 1829 (2002).
[45] M. I. Mishchenko and L. D. Travis, J. Quant. Spectrosc. Radiat. Transfer **60**, 309 (1998).
[46] J. C. Loudet, A. M. Alsayed, J. Zhang, and A. G. Yodh, Phys. Rev. Lett. **94**, 018301 (2005).